An Atomistic Perspective on the Effect of Strain Rate and Lithium Fraction on the Mechanical Behavior of Silicon Electrodes

Faezeh Darbaniyan
Department of Mechanical Engineering,
University of Houston,
Houston, TX 77004
e-mail: fdarbaniyan@uh.edu

Xin Yan[1]
School of Mechanical Engineering and Automation,
Beihang University,
Beijing 100091, China
e-mail: yan_xin@buaa.edu.cn

Pradeep Sharma[1]
Department of Mechanical Engineering,
University of Houston,
Houston, TX 77004;
Department of Physics,
University of Houston,
Houston, TX 77004;
Material Science and Engineering Program,
University of Houston,
Houston, TX 77004
e-mail: psharma@uh.edu

The process of charging and discharging of lithium-ion batteries results in the periodic intercalation and ejection of lithium ions in the anode material. High-capacity anode materials that are of significant interest for next-generation batteries, such as silicon, undergo large deformation during this process. The ensuing electro-chemo-mechanical stresses and accompanying microstructural changes lead to a complex state of inelastic deformation and damage in the silicon electrode that causes a significant capacity loss within just a few cycles. In this study, we attempt to understand, from an atomistic viewpoint, the mechanisms underlying the plasticity behavior of Si-anode as a function of lithiation. Conventional molecular dynamics simulations are of limited use since they are restricted to loading rates in the order of 10^8 s^{-1}. Practical charging-discharging rates are several orders of magnitude slower, thus precluding a realistic atomistic assessment of the highly rate-dependent mechanical behavior of lithiated silicon anodes via conventional molecular dynamics. In this work, we use a time-scaling approach that is predicated on the combination of a potential energy surface sampling method, minimum energy pathway, kinetic Monte Carlo, and transition state theory, to achieve applied strain rates as low as 1 s^{-1}. We assess and compare the atomistic mechanisms of plastic deformation in three different lithium concentration structures: $LiSi_2$, LiSi, and $Li_{15}Si_4$ for various strain-rates. We find that the strain rate plays a significant role in the alteration of the deformation and damage mechanisms including the evolution of the plastic deformation, nucleation of shear transformation zone, and void nucleation. Somewhat anomalously, LiSi appears to demonstrate (comparatively) the least strain rate sensitivity. [DOI: 10.1115/1.4045545]

Keywords: Li–ion battery, plasticity, electrode, low strain rate, autonomous basin climbing

1 Introduction

The motivation to study rechargeable Li-ion batteries requires little introduction, given the extensive and intensive research that has unfolded on this subject over the past several decades. They are expected to play an important part in future energy storage solutions and materials issues ranging from design of electrodes to the development of electrolytes are under scrutiny [1–3]. Silicon, in particular, is a promising anode candidate for lithium–ion batteries due to its exceptional capacity–more than 10 times of conventional carbon electrodes, availability, and well-developed manufacturing approaches [4,5]. However, silicon anodes are not as practical as carbon-based materials due to the significant loss of stability and capacity after just a few cycles of charging and discharge [6,7]. Silicon electrodes undergo a nearly 300% volumetric deformation during lithiation-delithiation cycles [8] accompanied by extensive plasticity and mechanical damage [9].

Due to the existence of several review articles on the subject of lithium-ion batteries, we avoid a detailed literature review and simply refer the reader to the following resources and references therein [4,10,11] and focus on just a subset of works that are most closely connected to the present study. Ab initio methods as well as conventional empirical force-field based molecular dynamics (MD) have been used to understand various aspects of electrode behavior. Some representative examples are Li diffusion [12], fracture [13], brittle-ductile transition [14], plasticity [15], void growth [16], among others. The time-scale limitation of conventional MD is well known [17–21]. The inherent limitation in the methodology allows the modeling of a few microseconds thus limiting loading rates to unrealistically high values of the order of 10^8 s^{-1}. This is in sharp contrast to the highly rate-dependent behavior of lithiated silicon electrodes as well as the orders of magnitude of slower strain rates the electrodes are subjected to in practice. Relatively speaking, very few works have attempted to use time-scaling approaches to understand plasticity and damage in lithiated silicon electrodes. This is understandable given that most existing time-scaling approaches [19] are hardly turn-key operations and are computationally extremely demanding. There are however some notable exceptions, Mendez et al. [22] recently used the so-called diffusive molecular dynamics to examine the process of lithiation in silicon nanopillars. Two of the co-authors of the present work, previously, have used a time-scaling approach based on the potential energy sampling method to understand both Li-ion diffusion and the unit plastic event in fully lithiated silicon nanostructues identifying the rotation of the shear transformation zones as the main dissipation mechanism [23,24].

This work builds up on our prior work that focused on the unit plasticity event in amorphous fully lithiated silicon nanostructures [24]. In practice, the fraction of lithium in amorphous silicon anode changes continuously during the charging and discharging process [25]. Accordingly, in the present work, we employ a time-scaling atomistic approach and investigate the plasticity and void nucleation behavior of amorphous (bulk) silicon as a function of lithiation fraction as well as strain rate. Our approach allows us to consider the strain rate as low as 1 s^{-1}, which is several orders of magnitude beyond the reach of conventional MD and is in line with experimental strain rates.

[1]Corresponding authors.

Manuscript received October 31, 2019; final manuscript received November 23, 2019; published online November 26, 2019. Assoc. Editor: Yonggang Huang.

2 Approach

We used a modified embedded-atom method potential, which was developed by Qu et al. [12] to describe the atomistic interaction among Si and Li atoms. We created the amorphous structure via a rapid quench process [16]. We first randomly insert a specific concentration of lithium atoms into a crystalline silicon structure. Then, the temperature is increased to 2500 K. After equilibrium for 300 ps, the system is quenched with a quenching rate of 4.4×10^{11} K s^{-1} to room temperature. Finally, we equilibrated the system at room temperature and zero pressure using the NPT ensemble. The amorphous structures after quenching are shown in Fig. 1, and they are the initial structures for our simulations. The dimensions of the cubic unit cells are 42.78 Å for $Li_{15}Si_4$, 39.66 Å for LiSi and 45.21 Å for $LiSi_2$. There are 4750 atoms in the sample of $Li_{15}Si_4$, 3936 atoms in LiSi and 5604 atoms in $LiSi_2$. The samples were uni-axially stretched in the x-direction during loading, and all simulations were conducted with periodic boundary conditions in all directions. Large-scale atomic/molecular massively parallel simulator (LAMMPS) was used to carry out the classical MD calculations [26], and the atomistic structures were visualized using OVITO [27].

To realize the slow loading rate, we adopted a time-scaling approach based on a potential energy surface sampling method, the so-called autonomous basin climbing approach (ABC) [28,29]. Further details of the approach may be found in the papers of its originators [30,31] and several others [32,33]. Accordingly, we provide only a highly abbreviated description here. First, the desired strain rate is chosen, and an incremental value of the strain is imposed on the system. For the given imposed strain increment, the potential energy surface (PES) is sampled extensively using the ABC algorithm. The sampling of the PES provides us the minima and saddle points of the PES, and hence the energy barriers between all pairs of the minima. The nature of the ABC algorithm is such that while the minima are accurately determined, the estimates of the energy barriers may be erroneous. To refine the barrier estimates, some suitable minimum energy pathway approach (e.g., nudged elastic band method–NEB) must be used. Kinetic Monte Carlo (KMC) is then used to evolve the system toward the most probable path.

The time for the system to transit from initial energy well to the selected minima is calculated by implementing the transition state theory:

$$\Delta t = [\nu \exp(-\Delta E/k_b T)]^{-1} \tag{1}$$

where ΔE, k_b, and T are the energy barrier, Boltzmann constant, and absolute temperature, respectively. In Eq. (1), ν is the hopping frequency [34,35], set as $\nu = 10^{13}$ s^{-1}. The obtained transition time multiplied by the chosen strain rate provides us with the increment of the strain for the next iteration, and the ABC/NEB/KMC cycle is repeated. Further details may be found in Ref. [36] and the review articles [20,33].

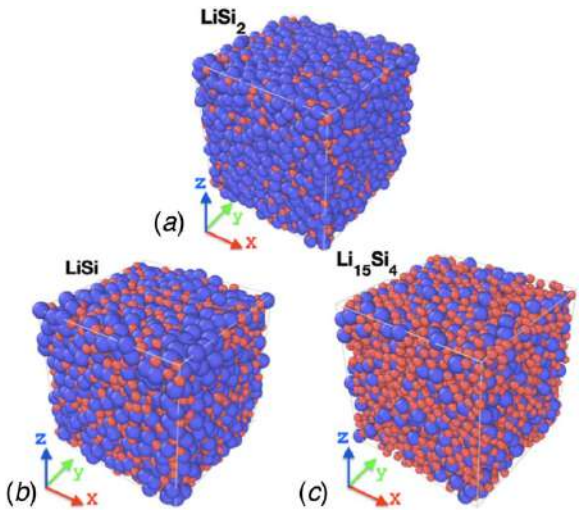

Fig. 1 Initial amorphous structures of (*a*) $Li_{15}Si_4$, (*b*) LiSi, and (*c*) $LiSi_2$. Large blue balls represent Si atoms and small red balls represent Li atoms.

3 Results and Discussion

We conducted the simulations for three different strain rates: 1 s^{-1} that is closer with experimental strain rates, 10^4 s^{-1}, and 10^8 s^{-1} that is accessible with conventional MD. We also carried out conventional MD simulations for the high strain rate case (10^8 s^{-1}) for benchmark comparison.

3.1 Comparison With Molecular Dynamics Results. For the high strain rate (10^8 s^{-1}) case, as evident from Fig. 2, ABC-based calculations and MD results are in reasonable accord. As fully expected (on physical grounds), the yield stress is lower for higher lithium concentration, and this has been documented by others as well e.g., Ref. [14].

3.2 The Effect of Strain Rate. To understand the effect of strain rate, the stress–strain curves of the each lithium fraction sample under different strain rates are shown in the same plot in Fig. 3. The snapshots during loading for $LiSi_2$, LiSi, and $Li_{15}Si_4$ together with the stress–strain curves are shown in Figs. 3(*a*)–3(*c*). There is a non-trivial drop in the yield stress with the reduction of strain rate, as fully expected and underscores the limitation of MD to make an accurate quantitative prediction under realistic experimental conditions. For example, in Fig. 3(*a*), the yield stress of $LiSi_2$ reduces from 10 GPa at the strain rate of 10^8 s^{-1} to 6.5 GPa at the strain rate of 1 s^{-1}. Similarly, in Fig. 3(*b*), the yield stress drops from (roughly) 8 GPa at the strain rate of 10^8 s^{-1} to 6 GPa at the strain rate of 1 s^{-1}.

To quantify the atomistics of plastic deformation, we examine the non-affine squared displacement of the atoms ($D^2_{\min}$) following the approach described in Refs. [37,38]. To evaluate this quantity, we take the initial structure as the reference configuration ($\mathbf{r}_i(0)$) and apply an affine transformation $\mathbf{J}_i$ to the reference distance vector ($\mathbf{r}_{ji}(0)$) between a designated center particle i and neighboring particles j. Assuming that there are N_i atoms within the cut-off distance, the non-affine squared displacement is then defined as [37]

$$D^2_{\min} = \frac{1}{N_i} \min_{\mathbf{J}_i} \sum_{j \in N_i} [\mathbf{r}_{ji}(t) - \mathbf{J}_i \mathbf{r}_{ji}(0)]^2 \tag{2}$$

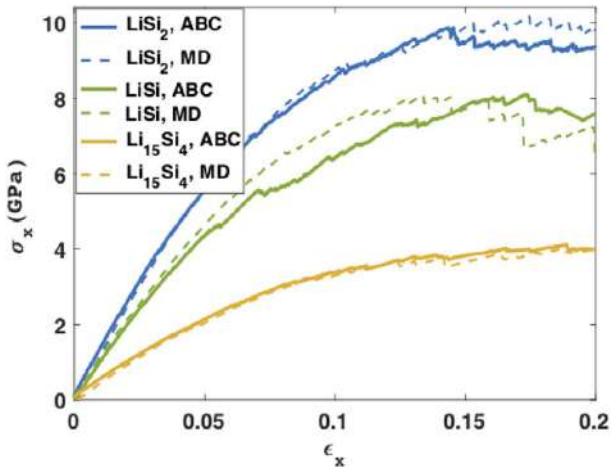

Fig. 2 Comparison of MD (dashed lines) and ABC (solid lines) uni-axial stress-strain curves for tensile test of same initial sample (created under quenching rate of 4.4×10^{11} K s^{-1}) and the strain rate of 10^8 s^{-1}. MD stretch was conducted at a temperature of 1 K. Here, blue, green, and yellow colors refer to $LiSi_2$, LiSi, and $Li_{15}Si_4$ structures accordingly.

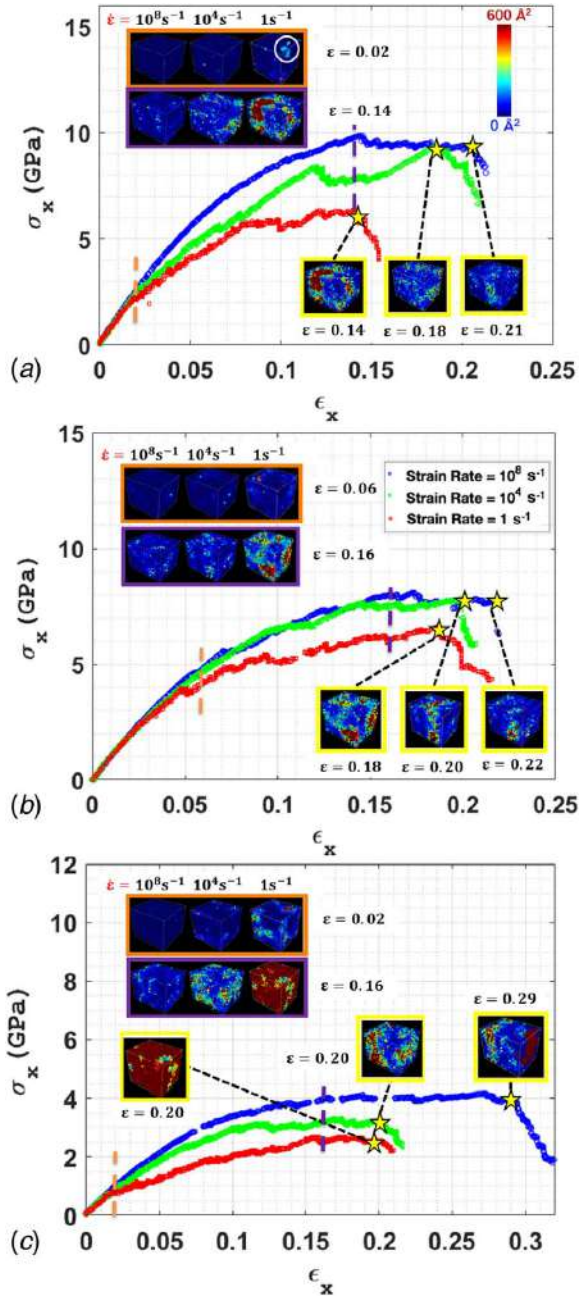

Fig. 3 Stress–strain curves at different loading rates for (*a*) $LiSi_2$, (*b*) LiSi, and (*c*) $Li_{15}Si_4$. (All the curves share the same legend shown in (*b*) and all the snapshots share the same color bar shown in (*a*).)

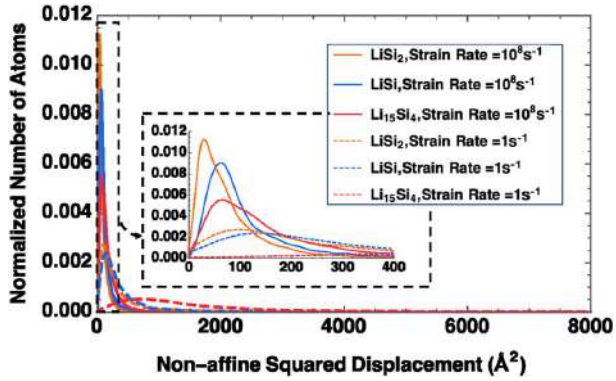

Fig. 4 Smoothed histogram plot of the number of atoms at each non-affine squared displacement value normalized with total atom numbers at onset of fracture (labeled with yellow stars in Fig. 3)

where $\mathbf{r}_{ji}(0) = \mathbf{r}_j(0) - \mathbf{r}_i(0)$ is the distance vector between atoms i and j and parentheses (t) and (0) correspond to the current time t and reference time, respectively. Thus, $D^2_{\min}$ is a measure of excess particle displacement and rearrangement with respect to the local (affine) shape change. The internal structure evolution shown in the snapshots Fig. 3 is colored based on the magnitude of the non-affine displacement ($D^2_{\min}$) value (all the snapshots share the same color bar which is shown in Fig. 3(*a*)). For $LiSi_2$ (Fig. 3(*a*)), we pick $\epsilon = 0.02$ and $\epsilon = 0.14$ for a closer scrutiny of the internal structure. As can be observed, for the samples at the strain of 0.02 (Fig. 3(*a*)), for the strain rates of $10^8\ s^{-1}$ and $10^4\ s^{-1}$, there is no discernible change in the internal structure. However, for the strain rate of $1\ s^{-1}$, even at a very early strain stage of $\epsilon = 0.02$, shear transformation zones (STZs) nucleate prominently (white circle). The implication is that even if MD were able to handle the reduction of strain rate to $10^4\ s^{-1}$ (which currently it cannot), the atoms barely participate in the rearrangement. At the strain of 0.14, STZ's are seen to be present for all strain rates; however, the size of STZs in the lower strain rate case, as well as values of $D^2_{\min}$, is larger. Similar observations may be made for other lithium-fraction samples.

An interesting observation in Fig. 3 is that at reduced strain rate, the system tends to initiate fracture at an earlier stage. The yellow stars indicate these fracture initiation points and the snapshots are shown in the yellow boxes. To understand the mechanism underpinning this observation, a smoothed histogram plot of the number of atoms at each non-affine squared displacement value normalized with total atom numbers at the onset of the fracture is shown in Fig. 4. The dashed lines depict the non-affine squared displacement distribution at the loading rate of $1\ s^{-1}$ and the solid lines indicate the variation of non-affine squared displacement value at the strain rate of $10^8\ s^{-1}$. The zoomed view of $D^2_{\min}$ varying from $0\ Å^2$ to $400\ Å^2$ is shown in the subset. We remark that even though high-strain rate loading cases appear to show fracture initiation at an earlier strain stage, it actually takes much longer physical time for slow loading case to nucleate voids. Taking $Li_{15}Si_4$ as an example, for high strain rate loading case ($10^8\ s^{-1}$), the time to void nucleation is 2.9 ns in comparison to 0.2 s for ($1\ s^{-1}$).

The number of atoms (lithium and silicon separately) for each span of non-affine squared displacement at the strain of 0.14 are shown in Fig. 5. At this level of strain, all lithiated samples have yielded. In Fig. 5, blue columns represent the number of silicon atoms and yellow columns stand for lithium. These graphs essentially underscore the larger content of non-affine displacement (and hence plastic events) at lower strain rates.

3.3 Effect of Li Concentration. Si is brittle, and as demonstrated in prior works, the Li atoms endow the apparent ductility seen in lithiated samples. The stress–strain behavior for varying lithiation is shown in Fig. 6. For all strain rates, $LiSi_2$ yields at the highest stress and the yields stress of $Li_{15}Si_4$ is much lower than the other two cases. At reduced strain rates, the behavior of $LiSi_2$ and LiSi becomes similar to each other, and they exhibit almost identical yield stress at the strain rate of $1\ s^{-1}$.

In order to obtain insights into the plasticity behavior of the different lithiated samples, in Fig. 7, we plot a histogram of the normalized number of atoms with respect to the value of non-affine squared displacement at the strain rate of $1\ s^{-1}$. Somewhat surprisingly, we observe an anomalous (non-monotonic) variation of non-affine displacement with respect to the lithiation fraction. LiSi exhibits the highest peak for low non-affine displacement instead of $LiSi_2$.

We speculate that the anomalous observation described in the preceding paragraph is likely associated with the higher density

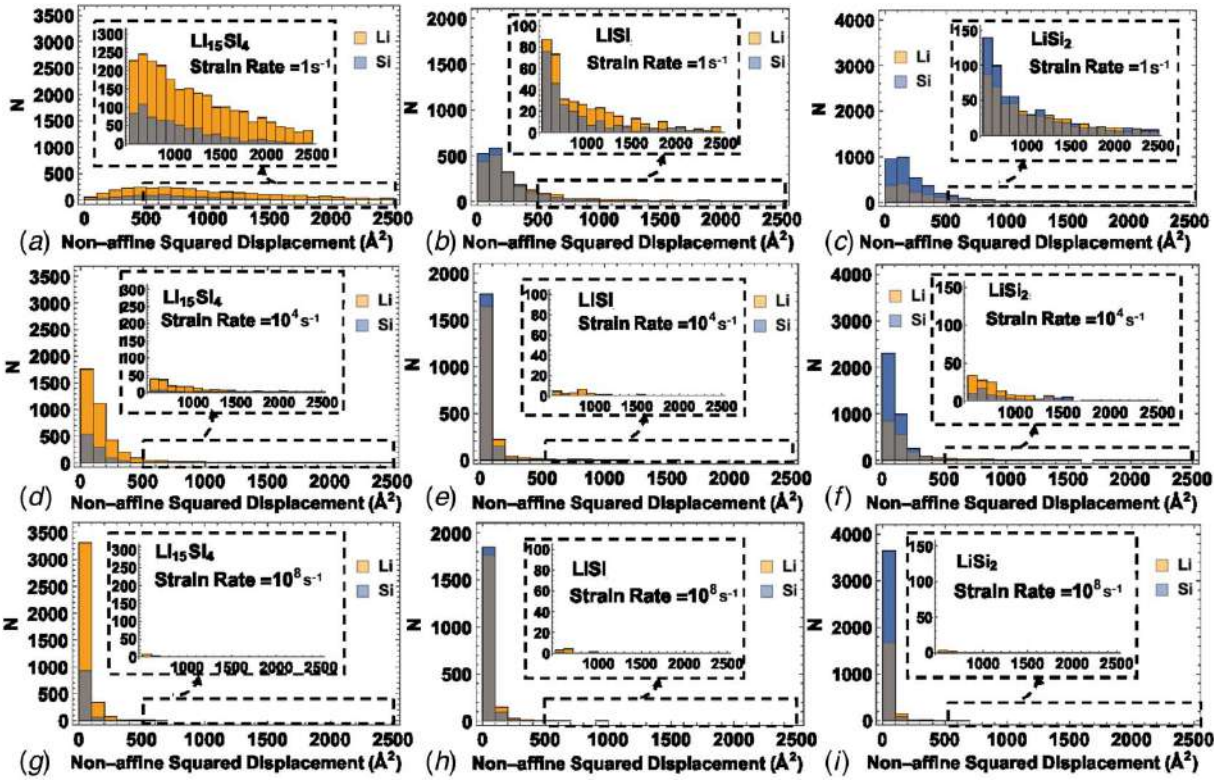

Fig. 5 Number of atoms for each non-affine squared displacement range at the strain of 0.14. Top, medium, and bottom row are for the strain rate of 1 s^{-1}, 10^4 s^{-1}, and 10^8 s^{-1}, respectively, and left, middle, and right columns correspond to $Li_{15}Si_4$, LiSi, and $LiSi_2$ structures, respectively.

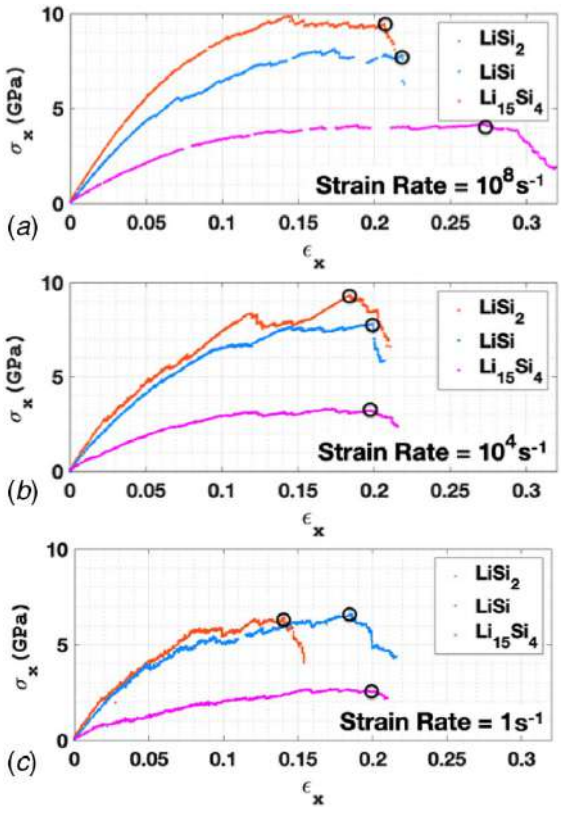

Fig. 6 Stress–strain curves for ABC simulations at the strain rate of (*a*) 10^8 s^{-1}, (*b*) 10^4 s^{-1}, and (c) 1 s^{-1}. Orange, blue, and pink correspond to $LiSi_2$, LiSi, and $Li_{15}Si_4$, respectively. Here, points marked with circles denote the initiation of fracture.

of Li–Si bonds in the LiSi structure. To explore this further, we carried out a bond analysis. The number of paired atomic bonds variation at strain rate of 1 s^{-1} is calculated and shown in Fig. 8. In order to restrict the effect of other parameters, the number of bonds is normalized with respect to the total number of bonds at an initial structure for each case. For two structures, $LiSi_2$ (Fig. 9(*a*)) and LiSi (Fig. 9(*b*)), the behavior of Li–Si bonds are qualitatively the same: the normalized number of Li–Si bond starts to reduce for both structures with the same rate at strain equals to 0.05. What changes between LiSi and $LiSi_2$ is the normalized number of Li–Li and Si–Si bonds. These bonds behave oppositely in these two structures—the number of Li–Li bonds for $LiSi_2$ is comparably negligible, similar to Si–Si bonds in LiSi. The main difference in the bonds between $LiSi_2$ and LiSi is the fact that $LiSi_2$ loses Si–Si bonds whereas LiSi loses Li–Li bonds. The weakness of Li–Li bond (metallic bond) compared with Si–Si (covalent bond) results into the softening of the structure during loading. Based on the previous investigation reported in Refs. [24,39], during the plastic deformation of Li–Si alloy, Si atoms build the frame and Li atoms are the "flowing defects" of the system. The breaking of Si–Si bonds is likely to affect the mechanical behavior more starkly compared with the breakage of Li–Li bonds. As a consequence of bond break, there is delayed plasticity initiation in LiSi when compared with $LiSi_2$ (Fig. 3). In Fig. 3(*a*), the plastic deformation initiates at an earlier strain level at around $\varepsilon = 0.02$ which is due to the bond breaking of both Li–Si bonds and Si–Si bonds (whose number is significantly lower from $\varepsilon = 0.02$). However, for LiSi, the main contribution comes from the breaking of Li–Si bonds which begins to happen at the strain stage around 0.05 (Fig. 8). In other words, the breaking of Si–Si bonds is more effective in reducing the stability of the sample than the fracture of Li–Li bonds. On the other hand, for $Li_{15}Si_4$, the number of Si–Si bonds are almost negligible and its behavior is dominated by the Li–Li and Li–Si bonds. Since Li–Li bonds are very weak and easily stretched, they can tolerate significant strain before breaking.

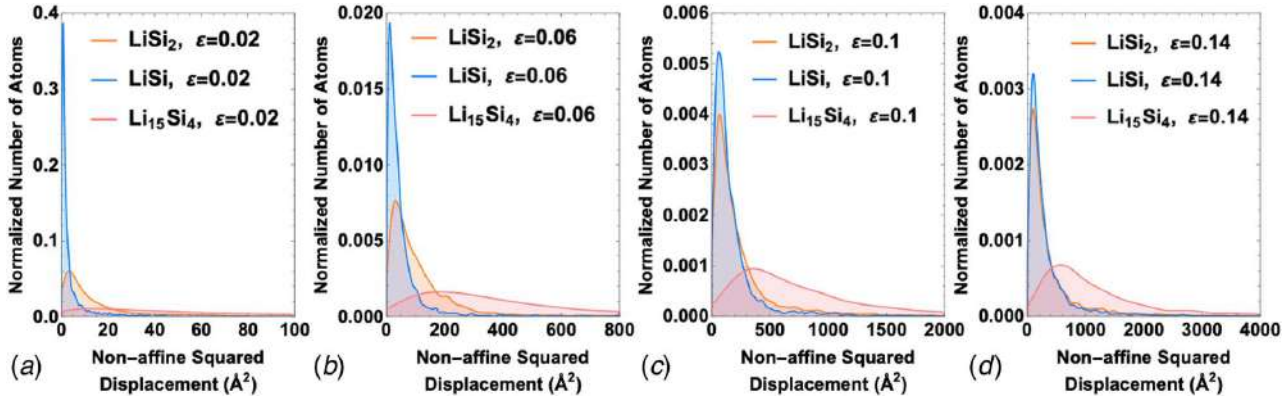

Fig. 7 Smoothed histogram plot of normalized atom number at varying non-affine squared displacement values for $\dot{\epsilon} = 1\ s^{-1}$. Plots denote the strain stage of (*a*) 0.02, (*b*) 0.06, (*c*) 0.1, and (*d*) 0.14, respectively.

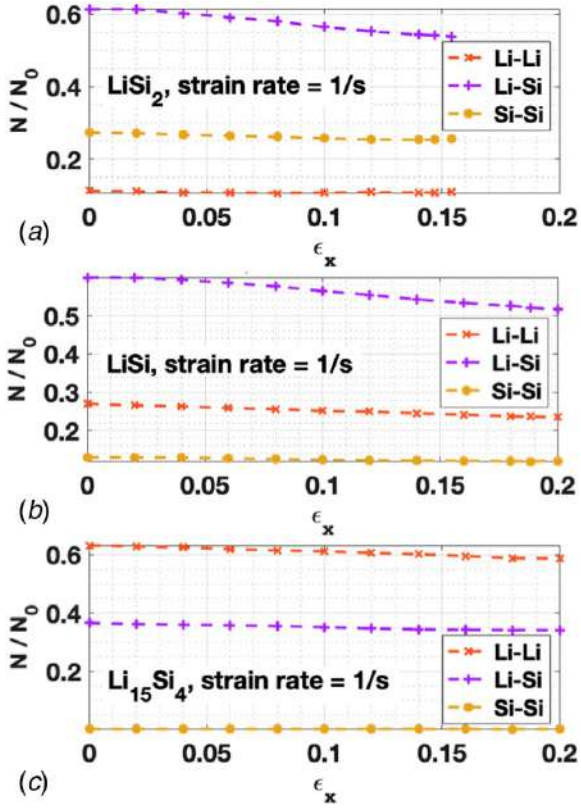

Fig. 8 Normalized bond number variation of loading at a strain rate of 1 s^{-1} for (*a*) $LiSi_2$, (*b*) LiSi, and (*c*) $Li_{15}Si_4$

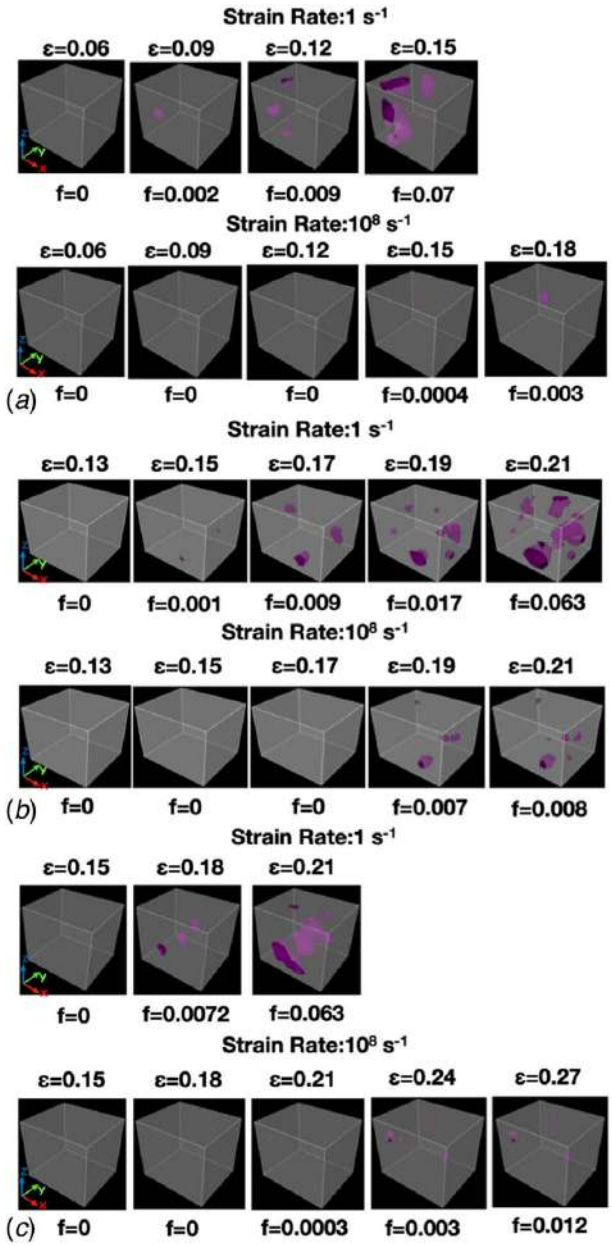

Fig. 9 Void nucleation of (*a*) $LiSi_2$, (*b*) LiSi, and (c) $Li_{15}Si_4$ at a strain rate of 1 s^{-1} (top lines) and 10^8 s^{-1} (bottom lines)

Breaking of Li–Si bonds is the main reason leading to void nucleation in $Li_{15}Si_4$. In short, at lower strain rates, increasing the lithium fraction does not necessarily soften the structure, and there exists an exception: LiSi shows less non-affine plasticity than $LiSi_2$.

3.4 Void Nucleation. Although a detailed examination of void nucleation and its underlying mechanistic underpinnings is beyond the scope of the present work, we perform a preliminary assessment of the onset of the fracture process. The void nucleation progression is shown in Fig. 9. The porosity f (labeled below every snapshots) is calculated using the void volume normalized with the total volume and is plotted in Fig. 10. From this figure, we can tell that the voids nucleate at different strain stages if the systems are loading in different rates. For example, in Fig. 9(*a*), the top line shows the void

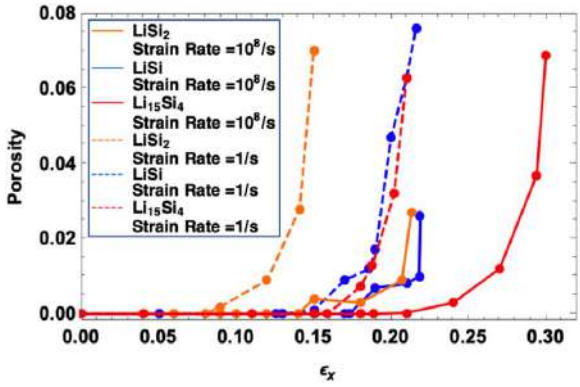

Fig. 10 Porosity variation versus strain for $LiSi_2$ (orange lines), LiSi (blue lines), and $Li_{15}Si_4$ (red lines) at the strain rate of 1 s^{-1} (dashed lines) and 10^8 s^{-1} (solid lines)

nucleation of $LiSi_2$ at the strain rate of 1 s^{-1} and the bottom line represents the variation at the strain rate of 10^8 s^{-1}. For the case of strain rate of 1 s^{-1}, the void nucleation occurs at the strain of 0.09, while when loading the system at strain rate of 10^8 s^{-1}, the void starts to nucleate at the strain of 0.18 at which point the slow loading case (top line) has already failed. A similar observation can be found in the other two samples: LiSi (Fig. 9(*b*)) and $Li_{15}Si_4$ (Fig. 9(*c*)). For LiSi (Fig. 9(*b*)), the void starts to nucleate at the strain of 0.15 for the slow loading case (1 s^{-1}) and at the strain of 0.19 for quick loading case (10^8 s^{-1}). In the following strain stages, the porosity f for slow loading case is always larger than the faster loading rate. For $Li_{15}Si_4$ (Fig. 9(*c*)), if the system is loaded slowly (1 s^{-1}), the void starts to nucleate before the strain state of 0.18 and the void starts to nucleate at the strain of 0.21 for high strain rate (10^8 s^{-1}). In general, void nucleation for slow strain rate cases occurs at an earlier strain level and in regions where atoms have higher non-affine displacements. As before, the inability of MD (or higher strain rate simulations) to make realistic predictions of damage under laboratory conditions is quite evident. However, further analysis is needed to delve deeper into the fracture mechanisms which we defer to a future study.

4 Concluding Remarks

In this study, using a time-scaling atomistic approach, we have investigated the effect of strain rate and lithiation fraction on the mechanical behavior of amorphous silicon. We are able to capture loading rates as low as 1 s^{-1} which is well beyond the capabilities of conventional MD. We specifically find that MD or high strain rate calculations severely suppress plastic deformation both quantitatively as well as alter the nature of microstructural re-arrangements during the deformation evolution. Void nucleation, i.e., the onset of fracture, also occurs at earlier strain levels for slower (more realistic) strain rates. With respect to Li-fraction, we find that more Lithium does not necessarily make the amorphous alloy monotonically more ductile. The actual response depends on the fraction of the various atomic bonds and their role in the deformation process. In particular, we find that anomalous behavior for an intermediate lithiated Li–Si system.

Acknowledgment

XY acknowledges support from Fundamental Research Funds for the Central Universities and National Natural Science Foundation of China (NSFC-11902014). XY acknowledges the insightful discussion with Dr. Haorang Wang. PS acknowledges support from the M.D. Anderson Professorship. The authors acknowledge the use of the Maxwell, Opuntia, and Sabine Cluster and the advanced support from the Core facility for Advanced Computing and Data Science at the University of Houston to carry out the research presented here.

References

[1] Li, M., Lu, J., Chen, Z., and Amine, K., 2018, "30 Years of Lithium-Ion Batteries," Adv. Mater., **30**(33), p. 1800561.
[2] Liu, Y., Zhu, Y., and Cui, Y., 2019, "Challenges and Opportunities Towards Fast-Charging Battery Materials," Nat. Energy, **4**(7), pp. 540–550.
[3] Ardebili, H., 2019, "A Perspective on the Mechanics Issues in Soft Solid Electrolytes and the Development of Next-Generation Batteries," ASME J. Appl. Mech., **87**(4), pp. 1–4.
[4] McDowell, M. T., Lee, S. W., Nix, W. D., and Cui, Y., 2013, "25th Anniversary Article: Understanding the Lithiation of Silicon and Other Alloying Anodes for Lithium-Ion Batteries," Adv. Mater., **25**(36), pp. 4966–4985.
[5] Chan, C. K., Peng, H., Liu, G., McIlwrath, K., Zhang, X. F., Huggins, R. A., and Cui, Y., 2008, "High-Performance Lithium Battery Anodes Using Silicon Nanowires," Nat. Nanotechnol., **3**(1), pp. 31–35.
[6] Zhang, S., Zhao, K., Zhu, T., and Li, J., 2017, "Electrochemomechanical Degradation of High-Capacity Battery Electrode Materials," Prog. Mater. Sci., **89**, pp. 479–521.
[7] Beaulieu, L. Y., Eberman, K. W., Turner, R. L., Krause, L. J., and Dahn, J. R., 2001, "Colossal Reversible Volume Changes in Lithium Alloys," Electrochem. Solid-State Lett., **4**(9), pp. A137–A140.
[8] Shi, F., Song, Z., Ross, P. N., Somorjai, G. A., Ritchie, R. O., and Komvopoulos, K., 2016, "Failure Mechanisms of Single–Crystal Silicon Electrodes in Lithium–Ion Batteries," Nat. Commun., **7**, p. 11886.
[9] Wang, X., Fan, F., Wang, J., Wang, H., Tao, S., Yang, A., Liu, Y., Chew, H. B., Mao, S. X., Zhu, T., and Xia, S., 2015, "High Damage Tolerance of Electrochemically Lithiated Silicon," Nat. Commun., **6**, p. 8417.
[10] Ma, D., Cao, Z., and Hu, A., 2014, "Si-Based Anode Materials for Li-Ion Batteries: A Mini Review," Nano-Micro Lett., **6**(4), pp. 347–358.
[11] Lu, J., Chen, Z., Pan, F., Cui, Y., and Amine, K., 2018, "High-Performance Anode Materials for Rechargeable Lithium-Ion Batteries," Electrochem. Energy Rev., **1**(1), pp. 35–53.
[12] Cui, Z., Gao, F., Cui, Z., and Qu, J., 2012, "A Second Nearest-Neighbor Embedded Atom Method Interatomic Potential for Li–Si Alloys," J. Power Sources, **207**(1), pp. 150–159.
[13] Khosrownejad, S. M., and Curtin, W. A., 2017, "Crack Growth and Fracture Toughness of Amorphous Li–Si Anodes: Mechanisms and Role of Charging/Discharging Studied by Atomistic Simulations," J. Mech. Phys. Solids, **107**, pp. 542–559.
[14] Ding, B., Li, X., Zhang, X., Wu, H., Xu, Z., and Gao, H., 2015, "Brittle Versus Ductile Fracture Mechanism Transition in Amorphous Lithiated Silicon: From Intrinsic Nanoscale Cavitation to Shear Banding," Nano Energy, **18**, pp. 89–96.
[15] Zhao, K., Wang, W. L., Gregoire, J., Pharr, M., Suo, Z., Vlassak, J. J., and Kaxiras, E., 2011, "Lithium-Assisted Plastic Deformation of Silicon Electrodes in Lithium-Ion Batteries: A First-Principles Theoretical Study," Nano Lett., **11**(7), pp. 2962–2967.
[16] Wang, H., Wang, X., Xia, S., and Chew, H. B., 2015, "Brittle-to-Ductile Transition of Lithiated Silicon Electrodes: Crazing to Stable Nanopore Growth," J. Chem. Phys., **143**, p. 104703.
[17] Rodney, D., Tanguy, A., and Vandembroucq, D., 2011, "Modeling the Mechanics of Amorphous Solids at Different Length Scale and Time Scale," Modell. Simul. Mater. Sci. Eng., **19**(8), p. 083001.
[18] Voter, A. F., Montalenti, F., and Germann, T. C., 2002, "Extending the Time Scale in Atomistic Simulation of Materials," Annu. Rev. Mater. Res., **32**(1), pp. 321–346.
[19] Henkelman, G., Jónsson, H., Lelièvre, T., Mousseau, N., and Voter, A. F., 2018, *Handbook of Materials Modeling: Methods: Theory and Modeling*, Springer, pp. 1–10.
[20] Fan, Y., and Cao, P., 2018, *Handbook of Materials Modeling: Applications: Current and Emerging Materials*, Springer, pp. 1–27.
[21] Hammami, F., and Kulkarni, Y., 2017, "Rate Dependence of Grain Boundary Sliding Via Time-Scaling Atomistic Simulations," J. Appl. Phys., **121**(8), p. 085303.
[22] Mendez, J. P., Ponga, M., and Ortiz, M., 2018, "Diffusive Molecular Dynamics Simulations of Lithiation of Silicon Nanopillars," J. Mech. Phys. Solids, **115**, pp. 123–141.
[23] Yan, X., Gouissem, A., and Sharma, P., 2015, "Atomistic Insights Into Li-Ion Diffusion in Amorphous Silicon," Mech. Mater., **91**, pp. 306–312.
[24] Yan, X., Gouissem, A., Guduru, P. R., and Sharma, P., 2017, "Elucidating the Atomistic Mechanisms Underpinning Plasticity in Li–Si Nanostructures," Phys. Rev. Mater., **1**(5), p. 055401.
[25] Li, J., and Dahn, J. R., 2007, "An In Situ X-Ray Diffraction Study of the Reaction of Li With Crystalline Si," J. Electrochem. Soc., **154**(3), pp. A156–A161.
[26] Plimpton, S., 1995, "Fast Parallel Algorithms for Short-Range Molecular Dynamics," J. Comput. Phys., **117**(1), pp. 1–19.
[27] Stukowski, A., 2010, "Extracting Dislocations and Non-Dislocation Crystal Defects From Atomistic Simulation Data," Modell. Simul. Mater. Sci. Eng., **18**(8), p. 085001.
[28] Kushima, A., Lin, X., Li, J., Eapen, J., Mauro, J. C., Qian, X., Diep, P., and Yip, S., 2009, "Computing the Viscosity of Supercooled Liquids," J. Chem. Phys., **130**(22), p. 224504.

[29] Kushima, A., Lin, X., Li, J., Qian, X., Eapen, J., Mauro, J. C., Diep, P., and Yip, S., 2009, "Computing the Viscosity of Supercooled Liquids. II. Silica and Strong-Fragile Crossover Behavior," J. Chem. Phys., **131**(16), p. 164505.
[30] Kushima, A., Eapen, J., Li, J., Yip, S., and Zhu, T., 2011, "Time Scale Bridging in Atomistic Simulation of Slow Dynamics: Viscous Relaxation and Defect Activation," Eur. Phys. J. B, **82**(3–4), p. 271.
[31] Fan, Y., Kushima, A., and Yildiz, B., 2010, "Unfaulting Mechanism of Trapped Self-Interstitial Atom Clusters in Bcc Fe: A Kinetic Study Based on the Potential Energy Landscape," Phys. Rev. B, **81**(10), p. 104102.
[32] Cao, P., Yoon, G., Tao, W., Eom, K., and Park, H. S., 2015, "The Role of Binding Site on the Mechanical Unfolding Mechanism of Ubiquitin," Sci. Rep., **5**, p. 8757.
[33] Yan, X., Cao, P., Tao, W., Sharma, P., and Park, H. S., 2016, "Atomistic Modeling at Experimental Strain Rates and Timescales," J. Phys. D: Appl. Phys., **49**(49), p. 493002.
[34] Voter, A. F., 2007, *Radiation Effects in Solids: Introduction to the Kinetic Monte Carlo Method*, Springer, pp. 1–23.
[35] Nguyen, L. D., Baker, K. L., and Warner, D. H., 2011, "Atomistic Predictions of Dislocation Nucleation With Transition State Theory," Phys. Rev. B, **84**(2), p. 024118.
[36] Fan, Y., Osetskiy, Y. N., Yip, S., and Yildiz, B., 2013, "Mapping Strain Rate Dependence of Dislocation-Defect Interactions by Atomistic Simulations," Proc. Natl. Acad. Sci. U.S.A, **110**(44), pp. 17756–17761.
[37] Li, W., Rieser, J. M., Liu, A. J., Durian, D. J., and Li, J., 2015, "Deformation-Driven Diffusion and Plastic Flow in Amorphous Granular Pillars," Phys. Rev. E, **91**(6), p. 062212.
[38] Shimizu, F., Ogata, S., and Li, J., 2007, "Theory of Shear Banding in Metallic Glasses and Molecular Dynamics Calculations," Mater. Trans., **48**(11), pp. 2923–2927.
[39] Zhao, K.-J., Li, Y.-G., and Brassart, L., 2013, "Pressure-Sensitive Plasticity of Lithiated Silicon in Li-Ion Batteries," Acta. Mech. Sin., **29**(3), pp. 379–387.